

Fast Quench Detection in SFCL Pancake Using Optical Fibre Sensing and Machine Learning

A. Akbar¹, *PhD Student*, and B. Dutoit¹, *Senior Scientist*

¹SCI-IC-BD, École Polytechnique Fédérale de Lausanne, Lausanne, CH-1015, Switzerland

Abstract— A fast hotspot detection technique has been implemented and patented at École Polytechnique Fédérale de Lausanne (EPFL) under the European Union project FastGrid. The optical fibre sensing based technique uses the Mach-Zehnder Interferometer (MZI) and can detect even singular hotspots in the superconductor within 15ms. The MZI setup is very sensitive to external perturbations and mechanical stresses, which can manifest in the output along with the response to hotspots. The disturbance the setup is subject to, varies with the sample being tested and the environment it is being tested in. For example, the sample length and configuration, in addition to the routing of the optical fibre can determine the extent of the stresses on the optical fibre. Previous publications, showcased experiment results on relatively simple sample configurations which were straight HTS tapes with short lengths (0.3m or 1m). This manuscript will investigate the technique feasibility for a more complicated sample type: a pancake prototype for a superconducting fault current limiter (SFCL), comprising 12m of HTS tape in a bifilar winding, with taped optical fibre along the length of the conductor. The manuscript will also give a brief overview of a machine learning based post processing technique for the experimental data, developed at EPFL to supplement the MZI based quench detection for easy and reliable quench detection in large scale applications.

Index Terms— SFCL, quench detection, hotspot detection, optical fibre sensing, Mach-Zehnder Interferometer, HTS

I. INTRODUCTION

THE climate change phenomena has brought with it the urgency to switch to green energy. According to the global outlook shared in the International Energy Agency (IEA) report, the share of renewables in total electricity generation will globally increase from 29% in 2020 to over 60% in 2030 and to nearly 90% in 2050 [1]. This will bring with it the need for a more efficient mechanism to efficiently connect remote renewable energy generation sites to the demand sites. The International Renewable Energy Agency (IRENA) has presented supergrids as a possible solution [2]. Supergrids are a large transmission network transmitting high-voltage DC (HVDC) with 30- 40% lower line losses as compared to AC transmission [2]. However, the lack of phase information makes fault detection challenging in supergrids [3].

A. Akbar (*the corresponding author*) is with the Applied Superconductivity Group, École Polytechnique Fédérale de Lausanne, Lausanne, CH-1015, Switzerland (e-mail: arooj.akbar@epfl.ch).

B. Dutoit is the head of the Applied Superconductivity Group, École Polytechnique Fédérale de Lausanne, Lausanne, CH-1015, Switzerland (e-mail: bertrand.dutoit@epfl.ch).

This solution therefore, comes with the obstacle of grid protection that must be overcome before deployment. SFCLs, are potential candidates that can help protect supergrids. SFCLs can transition rapidly from their superconducting dormant state to resistive state in the case of high fault currents, protecting the power line. However, before SFCLs can be used in a grid, the superconductor in the device has to be protected from hotspots which result due to the inhomogeneity of critical current along the length of the superconductor. The critical current is the current at which the superconductor transitions to resistive state. The inhomogeneity causes different points in the superconductor to transition at different current values. This can result in localized points of heating (hotspots) in the SFCL device which can evolve into thermal runaways if they go undetected, causing device damage. A reliable technique is there required to monitor hotspots in a SFCL device. Since electronic quench detection methods are not suitable for high voltage power devices, optical fibre sensing is an attractive alternative for the health monitoring of HTS power applications. There are numerous fibre optic based quench detection techniques that are being investigated for superconducting applications like Fibre Bragg, Raman based fibre sensors and Rayleigh backscattering [4]–[7]. However, the quench detection time for these methods is not fast enough to protect the SFCL device from hotspots. At EPFL under the FastGrid project, a fast optical fibre based hotspot detection technique has been patented [8]–[10]. This MZI technique is an extremely fast and economical way of detecting even singular points of heating in the superconductor within 15ms, making it a faster and cheaper alternative to existing optical fibre detection techniques.

The MZI technique has been successfully tested on short HTS sample lengths up to 1m, demonstrating the fast response and high sensitivity to hotspots [11], [12]. However, the MZI method is extremely sensitive to mechanical perturbations which makes it challenging to use the method on longer samples or samples with complicated configurations requiring bigger, noisier experimental setups. Testing the MZI technique on longer lengths of HTS tapes and in noisier setups is important for a better understanding of the extent of these challenges and to optimize the technique operability for large scale HTS applications. In this manuscript, the MZI experimental results will

be shown for a small SFCL pancake comprising 2x6m conductors in a bifilar winding configuration with optical fibre integrated along the whole length by means of an adhesive tape Kapton®. The manuscript will show the experiment results for this pancake, discuss the challenges of understanding the MZI response, and the post processing of the experimental data using machine learning to determine the feasibility of the MZI technique for the SFCL pancake.

II. THE MACH-ZEHNDER METHOD

A. Working Principle

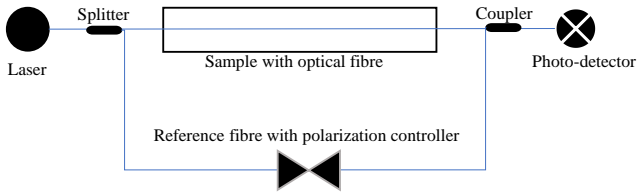


Fig. 1. The simple MZI setup for quench detection in HTS samples

The MZI technique requires a simple setup shown in Fig. 1 comprising laser source, splitter, coupler, photo-detector and two optical fibres. One fibre is integrated with the sample while the other fibre constitutes the reference arm of the interferometer. A polarization controller is present on the reference arm to align the polarization of light in both arms to ensure maximum peak to peak amplitude in the output interference pattern. Light is split into the two optical fibres at the input via the splitter and recombined at the output via the coupler where interference occurs. The MZI output at the photo-detector (i.e. the interference pattern) can be expressed as :

$$\text{Interference Pattern} \propto [1 + \cos(\phi_{12} - \pi + \Delta\phi_H)] \quad (1)$$

$$\Delta\phi_H \propto \{ (1 - \rho_a)\Delta\varepsilon + [\alpha_o + \xi]\Delta T \} \quad (2)$$

Where ϕ_{12} is the initial phase shift between the two light paths and $\Delta\phi_H$ is the phase shift due to hotspot plus ambient factors; as shown in Eq. (2) $\Delta\phi_H$ depends on the change in strain ($\Delta\varepsilon$) and temperature change (ΔT) experienced by the optical fibre [13], where ρ_a , α_o and ξ , are the photo-elastic coefficient, thermal expansion coefficient, and thermo-optic coefficient of the optical fibre respectively. Together the strain and temperature contribution (as apparent in Eq. (2)) define the MZI response sensitivity.

In the absence of a hotspot, both temperature and strain contributions arise due to environmental perturbations (like temperature, acoustic noise, and vibrations), which causes a slow variation of $\Delta\phi_H$. Hence, the MZI output in this case, exhibits slow fluctuations without any evident pattern. However, in the presence of a hotspot in the superconductor, the resulting temperature rise subjects the fibre to a temperature change while the thermal expansion of the Hastelloy imposes a



Fig. 2. The small SFCL pancake prototype comprising two conductors (1 and 2) in a bi-filar winding co-wound with three optical fibres on each conductor. There are five turns per conductor with insulating spacer between turns visible in the photo. One optical fibre on each conductor is spliced on both ends of each conductor (the external end fibres visible in blue and internal end spliced fibres visible in red, for each conductor)

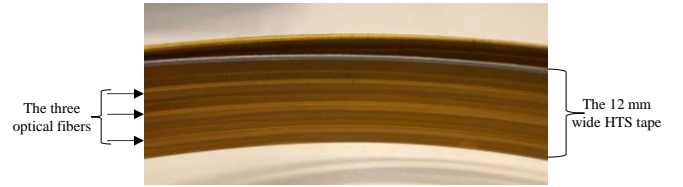


Fig. 3. A close look at how the three optical fibres are integrated with each conductor on the pancake by means of an adhesive tape Kapton® which is visible in yellow on top of the HTS tape

strain change on the optical fibre. The two terms in Eq. (2) increase and $\Delta\phi_H$ continuously increments from 0 to 2π , within few ms, in response to the hotspot. The rapid change in $\Delta\phi_H$ is visible at the MZI output as rapid, continuous periodic amplitude variations between 0 and 1V (normalized), which signals the presence of (at least) a single hotspot.

III. EXPERIMENT PROCEDURE

A. The SFCL Pancake

In the course of the FASTGRID project, a small pancake was hand wound at SuperGrid Institute (SGI), Lyon using a 12mm wide Theva tape with no shunt. The tapestar measurements for this conductor are not available hence the critical current is not specified. The pancake was made of 2x6m conductors (five turns per conductor) and three optical fibres were co-wound with each conductor using Kapton® at SGI. The optical fibre was present along the entire conductor length. An insulating spacer tape was also present in between the turns. This pancake

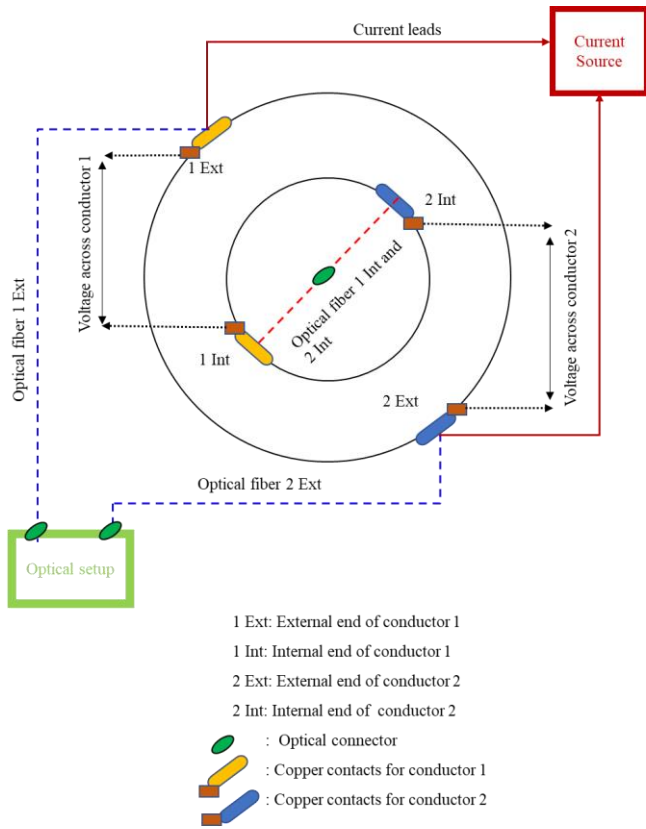


Fig. 4. The experiment setup schematic for testing the pancake, showing the optical as well as the electrical connections. The optical fibre on the two conductors were connected in series for an overall monitoring of the pancake for hotspots. The two conductors were connected in series to a DC current pulser and voltage across both conductors was acquired.

is shown in Fig. 2, where the labels for the two conductors (conductor 1 and conductor 2) internal ends (labelled *int*) and external ends (labelled *ext*) are visible. Three optical fibres were used to add redundancy in case any optical fibre broke during the winding and integration process. Fig. 3 shows how the three optical fibres are integrated on each pancake conductor by means of an adhesive tape (Kapton®). At the conductor ends 1m of free fibre was left, to enable easy splicing (connection) to the optical setup which was present externally and not part of the pancake. Only one optical fibre is spliced per conductor, the two ends of the spliced fibre for each conductor are also visible in Fig. 2 in red and blue.

B. Experiment Setup

The two conductors (1 and 2) are connected in series to a DC current source along with a current measurement shunt of $1\text{m}\Omega$. Voltage measurement taps were placed at the copper contacts for overall voltage measurement in the two conductors. One of the three optical fibres on each conductor was spliced to FC/APC connector cables and the optical fibre on the two conductors was connected in series, then connected to the optical fibre setup present externally

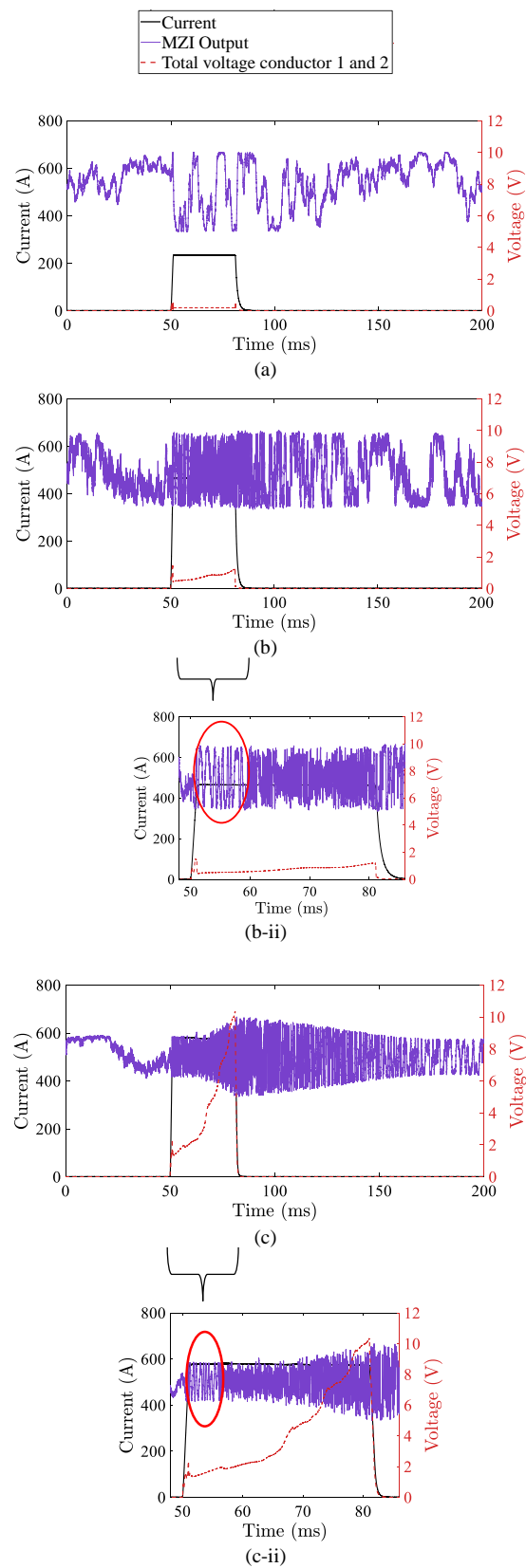


Fig. 5. The experiment results for the pancake, showing non-ideal MZI output cases which necessitate the need for machine learning: (a) oscillations in the absence of hotspots, (b) and (c) showcasing degrading oscillation quality after the initial good quality quench signal, (b-ii) and (c-ii) showing a zoomed in graph for (b) and (c) respectively to highlight the initial good quench signal important for data analysis.

as shown in Fig. 4. It is important when testing longer lengths that both arms of the MZI interferometer have the same lengths of optical fibre in order to retain coherence and ensure maximum peak to peak amplitude in the voltage at the photo-detector. The pancake was cooled to 77K in a liquid Nitrogen bath and 30ms pulsed current measurements were performed on the pancake with currents ranging up to 700A. The current, total pancake voltage and MZI output voltage were acquired.

IV. EXPERIMENT RESULTS AND MOTIVATION FOR MACHINE LEARNING

Experiment results for the pancake are plotted in Fig. 5. The graphs show the pulsed current in the pancake in black, the overall voltage in the pancake (sum of voltage in both conductors 1 and 2) in red. The voltage curves in Fig. 5 have an initial peak and non-zero value due to the circuit inductance. The MZI output voltage is shown in purple (scaled and shifted in the y-scale for plotting reasons as the variation is of importance and not the voltage value). The plots shown here are deliberately selected to showcase the problems that can occur when the MZI is used to detect hotspots in long conductor lengths and noisy setups. Fig. 5(a) shows how the MZI output is showing some form of oscillations even in the absence of any voltage in the sample; this can be due to bubbling in the cryostat, Lorentz force and other mechanical vibrations in the setup. These disturbances are manifesting in the MZI response, hence we observe these oscillations in the absence of hotspot, which may lead to false alarms. Fig. 5(b) and (c) show the MZI response to low heating and high heating in the pancake respectively. The MZI output can be seen to transition from a relatively slow fluctuation pattern to rapid amplitude variation as the voltage begins to rise in the sample however, it can be seen in the zoomed in graphs Fig. 5(b-ii) and (c-ii) that the oscillations become less clear and more noisy after the first 10ms. This can occur due to the disturbances introducing polarization rotation in the optical fibre leading to a loss of coherence, which is more noticeable in longer sample lengths [14]–[16]. It is however important to note that the initial quench signal is present within 10ms of the quench and is easily identified in the MZI output (as circled in red in Fig. 5(b-ii) and (c-ii)), signifying that the MZI is effectively monitoring hotspots in the pancake. It should be noted here, that even though the voltage measurements are apparent soon after the quench, they are not a feasible way for hotspot detection in large scale high voltage and inductive setups due to the presence of stray electric fields, inductive voltages and noise [17]. Therefore, non-electronic quench detection methods are suitable and preferred for HTS power applications.

These experiment results signify the need for a suitable data analysis technique, especially for big noisy setups, due to the possibility of false alarms and difficulty in visually analyzing the quench signal. Since the disturbances and their effect on the MZI output is difficult to determine and quantify and varies with the setup, the problem is of the form of a black-box, where the inputs and outputs are known but the internal working of the model is not fully known. This is why machine learning is a useful tool for the MZI setup, as it can help determine the

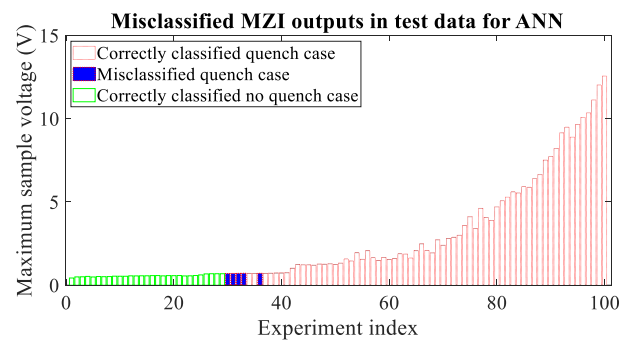


Fig. 6. A bar graph showing the spread of the test dataset ordered in terms of increasing voltage in the pancake. The graph also shows where the misclassified quench cases lie in the lower end of the quench cases.

process that links the inputs and outputs by means of classifiers like K-nearest neighbours (KNN) and Artificial Neural Networks (ANN) [18].

V. USING MACHINE LEARNING WITH EXPERIMENTAL DATA

A data analysis technique for reliable quench identification is a necessary and useful supplement to the MZI technique. A machine learning based quench classification method has been developed at EPFL for the MZI method, the details of which are available in this dedicated manuscript [19]. The data processing requires training the machine learning classifiers using a training dataset obtained from experiment measurements. The data set is the MZI output voltage normalized by the maximum voltage which is processed by means of Discrete Wavelet Transform and input to the training model. The trained classifiers are then used to classify a new test dataset also from the experiment measurements, to assign classification labels (quench or no quench) to each measurement. For each setup using the MZI method, training would be required as the disturbances will vary with the kind of environment MZI is being used in.

In the case of the pancake presented in this manuscript, a training dataset of 100 experiment measurements was used to train an Artificial Neural Network. ANN was used because of the variable and unquantifiable nature of the disturbances MZI experiences. ANN can help form a relationship with between the inputs and output labels without knowing the full working of the MZI method. This trained ANN was then tested on test dataset of 100 experiment measurements and the classification accuracy was determined. A quench classification accuracy of 95% was achieved with ANN on the experiment measurements obtained from the pancake.

The graph in Fig. 6 shows the 100 measurements from the test dataset ordered in terms of increasing heating. The shaded bars show where the misclassified measurements lie and it can be seen they lie in the low heating no-risk fault domain. All the high-risk quench cases are correctly classified by the classifier. It should be noted, that the low heating faults are present due to the pulsed measurements and in case of a real fault situation these faults will evolve into high heating faults and will be correctly classified by the ANN.

VI. CONCLUSION

This manuscript showcased experiment results for the MZI technique when used to monitor hotspots in a small SFCL pancake. Previously, the MZI technique feasibility was only demonstrated on simple linear HTS samples with short lengths (upto 1m). This manuscript is an important display of the MZI application not only to long lengths of HTS tapes but also for a SFCL module. While, the MZI detects a quench in the pancake almost immediately and within 10ms, there are possibilities of false alarms and poor-quality response. These results were used to highlight the need for a good data analysis technique to supplement the MZI setup, especially in larger and noisier superconducting applications. Machine learning based classification has been successfully implemented and tested with the pancake measurements giving a quench identification accuracy of 95%. The misclassified quench cases were low-heating no-risk scenarios which is a nudge in a promising direction for the MZI method, increasing its feasibility for quench detection in a range of superconducting applications. MZI is a significant breakthrough for superconducting applications as it provides an economical and fast way of quench detection. The next steps involve implementation of the data processing in real time, which will make it possible to deploy MZI on larger scales for extremely reliable quench detection, an innovation that will help overcome the superconductor health monitoring challenge.

REFERENCES

- [1] IEA, "Net Zero by 2050," 2021. doi: 10.1787/c8328405-en.
- [2] IRENA, "Innovation landscape brief: Supergrids," 2019.
- [3] W. Platzer and Fraunhofer ISE, "SUPERGRID – Approach for the integration of renewable energy in Europe and North Africa," p. 38, 2016, [Online]. Available: <https://www.ise.fraunhofer.de/en/publications/veroeffentlichungen-pdf-dateien-en/studien-und-konzeptpapiere/study-supergrid-fraunhofer-ise.pdf>.
- [4] A. Chiuchiolo *et al.*, "Fibre bragg grating cryosensors for superconducting accelerator magnets," *IEEE Photonics J.*, vol. 6, no. 6, pp. 1–10, 2014, doi: 10.1109/JPHOT.2014.2343994.
- [5] J. Jiang *et al.*, "Experimental Study on Quench Detection of a No-Insulation HTS Coil Based on Raman-Scattering Technology in Optical Fibre," *IEEE Trans. Appl. Supercond.*, vol. 28, no. 3, pp. 1–5, 2018, doi: 10.1109/TASC.2018.2802487.
- [6] F. Scurti, S. Ishmael, G. Flanagan, and J. Schwartz, "Quench detection for high temperature superconductor magnets: a novel technique based on Rayleigh-backscattering interrogated optical fibres," *Supercond. Sci. Technol.*, vol. 29, no. 3, p. 03LT01, Jan. 2016, doi: 10.1088/0953-2048/29/3/03lt01.
- [7] C. W. K. Schwartz Justin, Scurti Federico, Rogers Samuel, "United States Patent Application Publication Schwartz *et al.*," US 20170179364, 2017.
- [8] P. Tixador *et al.*, "Status of the european union project FASTGRID," *IEEE Trans. Appl. Supercond.*, vol. 29, no. 5, 2019, doi: 10.1109/TASC.2019.2908586.
- [9] Z. Y. Arooj Akbar, "Hotspot monitoring system for superconducting device," WO2021038505 (A1).
- [10] P. J. Tixador *et al.*, "Some results of the EC project FASTGRID," *IEEE Trans. Appl. Supercond.*, p. 1, 2022, doi: 10.1109/TASC.2022.3151318.
- [11] A. Akbar, Z. Yang, S. Wang, L. Thévenaz, and B. Dutoit, "Optical fibre sensing for fast hotspot detection in {SFCLs}," *Supercond. Sci. Technol.*, vol. 33, no. 11, p. 115003, Sep. 2020, doi: 10.1088/1361-6668/abb200.
- [12] A. Akbar, N. Riva, Z. Yang, L. Thevenaz, and B. Dutoit, "Fast Hotspot Detection in SFCLs by Exploiting Strain Response in Optical Fibre Sensing," *IEEE Trans. Appl. Supercond.*, vol. 31, no. 5, 2021, doi: 10.1109/TASC.2021.3061346.
- [13] A. D. Kersey *et al.*, "Fibre grating sensors," *J. Light. Technol.*, vol. 15, no. 8, pp. 1442–1462, 1997, doi: 10.1109/50.618377.
- [14] N. Imoto, N. Yoshizawa, J. Sakai, and H. Tsuchiya, "Birefringence in single-mode optical fibre due to elliptical core deformation and stress anisotropy," *IEEE J. Quantum Electron.*, vol. 16, no. 11, pp. 1267–1271, 1980, doi: 10.1109/JQE.1980.1070382.
- [15] G. Heise and R. Narevich, "Simple model for polarization sensitivity of silica waveguide Mach-Zehnder interferometer," *IEEE Photonics Technol. Lett.*, vol. 17, no. 10, pp. 2116–2118, 2005, doi: 10.1109/LPT.2005.854342.
- [16] K. Nagano, S. Kawakami, and S. Nishida, "Change of the refractive index in an optical fibre due to external forces," *Appl. Opt.*, vol. 17, no. 13, p. 2080, 1978, doi: 10.1364/ao.17.002080.
- [17] M. Marchevsky, "Quench Detection and Protection for High-Temperature Superconductor Accelerator Magnets," *Instruments*, vol. 5, no. 3, 2021, doi: 10.3390/instruments5030027.
- [18] K. A. Gaurav and L. Patel, *Machine Learning With R*. 2020.
- [19] A. Akbar, N. Riva, and B. Dutoit, "Optical fibre based quench detection in HTS applications using machine learning classifiers," *Phys. C Supercond. its Appl.*, vol. 593, p. 1354007, 2022, doi: <https://doi.org/10.1016/j.physc.2021.1354007>.